J Mater Sci: Mater Electron (2015) 26:3717–3721
DOI 10.1007/s10854-015-2890-x

Effect of $BaTiO_3$ doping on the structural, electrical and magnetic properties of $BiFeO_3$ ceramics

H. Y. Dai · J. Chen · T. Li · D. W. Liu · R. Z. Xue · H. W. Xiang · Z. P. Chen

Received: 8 January 2015 / Accepted: 27 February 2015 / Published online: 4 March 2015

Abstract $(1 - x)BiFeO_3$–$xBaTiO_3$ ($x = 0.00$, 0.10, 0.20, 0.25 and 0.30) ceramics have been fabricated by the solid state reaction method. The effects of $BaTiO_3$ (BTO) doping on the structural, electrical and magnetic properties of $BiFeO_3$ (BFO) ceramics have been investigated. It is found that BTO doping can affect the structure of the BFO ceramics, and the multiferroic properties of BFO ceramics can hence be improved. The XRD measurements reveal that the structure of BFO was changed from rhombohedral to pseudo-cubic and the impurity phases were decreased both due to BTO doping. Analysis of microstructure indicates that the BTO doping can hinder the grain growth. Electrical measurements show that BFO doping improves the ferroelectric property due to the significantly decrease of the electric leakage density and the oxygen vacancy concentrations. Magnetic measurements indicate that the antiferromagnetism behavior of BFO is turned into a weak ferromagnetism state by addition of BTO. The related mechanism is also discussed in the paper.

1 Introduction

Multiferroic materials that exhibit both ferroelectric and magnetic orders simultaneously have received considerable attention in recent years, because of their interesting fundamental physics and potential applications in multiple-state memories, electric field controlled ferromagnetic resonance devices, sensors and actuator devices, etc. [1, 2]. Bismuth ferrite, $BiFeO_3$ (BFO), is the only single-phase multiferroic material at room temperature so far discovered. BFO has a rhombohedrally distorted ABO_3-type perovskite structure which belongs to the R3c space group. It exhibits a higher ferroelectric Curie temperature (approximately 830 °C) and a higher antiferromagnetic ordering Neel temperature (approximately 370 °C), and thus has been studied extensively and became one of the most studied multiferroic materials in recent years due to its importance in fundamental research as well as in commercial applications [3–5].

Although BFO possess such interesting properties, its future application is severely limited due to some drawbacks in it [6–8]. One of the problems is the high large leakage current. Such a large leakage current density is usually caused by charge defects, non-stoichiometry, chemical valance fluctuation of Fe ions and impurity phases in BFO material which makes it difficult to gain a well-saturated ferroelectric hysteresis loop and a low dielectric loss [6–8]. On the other, the net magnetization of BFO is too small. The magnetic ordering is of G-type antiferromagnetic, having a spiral modulated spin structure with an incommensurate long-wavelength period of 62 nm. This spiral spin structure leads to cancellation of net macroscopic magnetization and prevents the observation of the linear magnetoelectric effect [6–8]. These problems have to be satisfactorily overcome before BFO can be regarded as an ideal multiferroic material. In order to overcome these problems, many attempts have been undertaken [6–8]. And it is quite encouraging to find that the multiferroic properties of BFO can be significantly enhanced through solid-state reaction followed by leaching out the impurity phases, applying high magnetic field, high-pressure synthesis, ion substitution and forming solid-state-solution with other perovskite type oxides, etc. [6–8].

H. Y. Dai · J. Chen · T. Li · D. W. Liu · R. Z. Xue · H. W. Xiang · Z. P. Chen (✉)
School of Physics and Electronic Engineering, Zhengzhou University of Light Industry, Zhengzhou 450002, China
e-mail: haiyangdai@163.com

Barium titanate, $BaTiO_3$ (BTO), is a classical ferroelectric material which was widely used in electronic devices such as high permittivity capacitors, infrared detectors or piezoelectric transducers due to its respective properties [9–11]. In our work, BTO was selected to prepare BTO doped BFO by solid-state reaction method followed by rapid liquid phase sintering. The structural, electrical and magnetic properties of $(1 - x)$BFO–xBTO ceramics were investigated in this paper.

2 Experimental details

The polycrystalline ceramic samples of $(1 - x)BiFeO_3$–$xBaTiO_3$ (x = 0.00, 0.10, 0.20, 0.25 and 0.30) were prepared by solid state reaction method followed by rapid liquid phase sintering. Pure BFO and BTO were synthesized according to stoichiometric ratio. Compared with conventional solid-state reaction method, the rapid liquid phase sintering can accelerate the synthesizing reaction, prevent the volatilization of Bi^{3+}, and suppress the formation of oxygen vacancies, Fe^{2+} ions and second phases. And with high heating rate and short period sintering, the appearance of the liquid phase will accelerate the synthesizing reaction during the synthesizing reaction helping to improve the crystal quality. The BFO ceramic powder was synthesized by the solid state reaction method followed by rapid liquid phase sintering [12] and the BTO ceramic powder was prepared by the traditional solid state reaction method using $BaCO_3$ and TiO_2 powders as starting materials. The synthesized BFO and BTO ceramics were used as raw materials to synthesize $(1 - x)$BFO–xBTO. The stoichiometric amount of BFO and BTO were mixed and thoroughly reground by using agate mortar for 2 h to form a uniform dispersive composite and then calcined at 700 °C for 4 h in air. The calcined powders, after pressed into pellets with a diameter of 10 mm and thickness of 2 mm, were sintered at 930–960 °C with an accuracy of ±1 °C for 30 min. After that they were taken out of the furnace immediately and quenched subsequently to room temperature. To measure the electrical properties of the samples, the disks were carefully polished and coated with silver paste on both sides as electrodes, and then fired at 600 °C for 30 min for measurement of the electric properties.

The crystal structure of samples was analyzed by X-ray diffraction (XRD, Bruke D8 Adcance) with Cu-Kα radiation. The morphologies of the samples were carried out in a scanning electron microscope (SEM, FEI Quanta200). The leakage current and ferroelectric properties samples were measured using ferroelectric tester (RT 6000, Radient Technology, USA) at room temperature. The magnetization of the samples was measured by a vibrating sample magnetometer integrated in a magnetic property measurement system (MPMS, Quantum Design).

3 Results and discussion

Figure 1 shows the XRD patterns of $(1 - x)$BFO–xBTO ($x = 0.00$–0.30) solid solutions at room temperature. The diffraction peaks of the undoped BFO can be identified as a rhombohedrally distorted perovskite structure with a space group of R3c. From the XRD analysis, it can be observed that the sintered $(1 - x)$BFO–xBTO ceramics exhibit well crystallized diffraction patterns and has a majority phase of BFO. A few small traces of impurity were observed in the case of $x = 0.00$–0.30, which were found to be those of $Bi_2Fe_4O_9$ and $Bi_{25}Fe_2O_{39}$ (labeled by a star in Fig. 1) [13, 14]. It is also found that the impurity phases in $(1 - x)$BFO–xBTO ceramics decrease with increasing BTO content, and they almost disappear in the x = 0.30 sample. It means that the BTO doping can hinder the formation of impurity phases in BFO. The reasons may be that BTO in the solid solution can accelerate the formation of BFO, eliminate oxygen vacancies, avoid compositional fluctuations of Fe^{3+} to Fe^{2+} oxidation, and stabilize the perovskite BFO phase. The diffraction peaks in the pattern of $x = 0.10$ and 0.20 samples shift slightly toward lower angle compared with those of undoped BFO ceramic. The shift of diffraction peaks implies that the $x = 0.10$ and 0.20 samples maintain the same rhombohedral structure as that of undoped BFO ceramic, and the doping of BTO induces the crystal structure distortion, such a distortion becomes serious with increasing the amount of doped BTO. This also indicates that BTO as a solid solution in the BFO phase leads to compressing the lattice and induces the

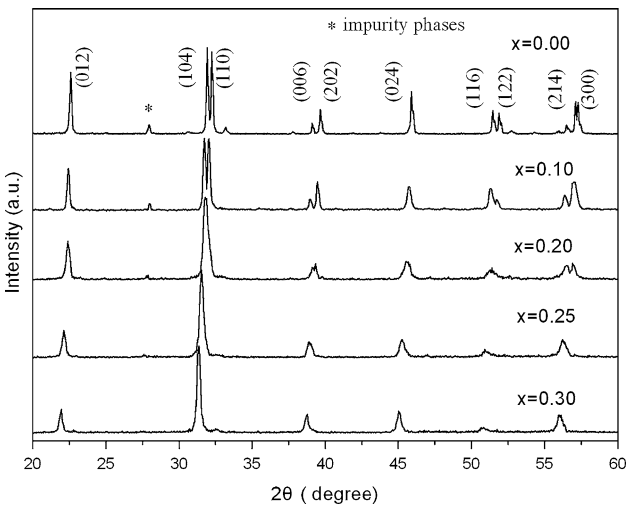

Fig. 1 XRD patterns of $(1 - x)BiFeO_3$–$xBaTiO_3$ samples

lattice constant smaller than that of undoped BFO. With increasing the concentration of BTO from $x = 0.20$ to 0.30, a gradual change towards a pseudo-cubic symmetry with the BTO addition is proved by gradual cancellation of the splitting of the diffraction peaks such as (104) and (110); (006) and (202) peaks in Fig. 1. This change in XRD pattern may be attributed to that the ionic radius of Ba^{2+} (1.35 Å) is larger than that of Bi^{3+} (1.03 Å) on the A site, but the Ti^{4+} ion (0.605 Å) and Fe^{3+} ion (0.64 Å) have similar ionic radius on the B site [10, 15].

Figure 2 shows the SEM images of the $(1 - x)$BFO–xBTO samples. Significant changes in the microstructure of the $(1 - x)$BFO–xBTO ceramics can be clearly observed. For the undoped sample shown in Fig. 3a, large grains with spherical pores inside the grains can be found, which appeared to grow abnormally or discontinuously. The morphology of the BTO doped samples becomes dense and uniform. With increasing the BTO doping content x from 0.00 to 0.30, the average grain size decreases as shown in Fig. 3b–e. The decrease in grain size might be interpreted in terms of suppression of oxygen vacancies concentration, which slows oxygen ion motion and consequently grain growth. In our case, the Ti^{4+} ions play a role of donor in BFO because the valance of Ti^{4+} is higher than that of Fe^{3+} ions, and charge imbalance may be compensated by filling the oxygen vacancies created due to valence state fluctuation between Fe^{3+} and Fe^{2+} [16]. In addition, since the strength of Ba–O bond (563 ± 42 kJ/mol) is higher than that of Bi–O bond (343 ± 6 kJ/mol) [17], the substitution of Ba for Bi in the A site can stabilize the perovskite structure, decrease the volatilization of Bi, lower the concentration of oxygen vacancies. Therefore, a suppressed oxygen vacancy due to BTO doping inhibits the grain growth.

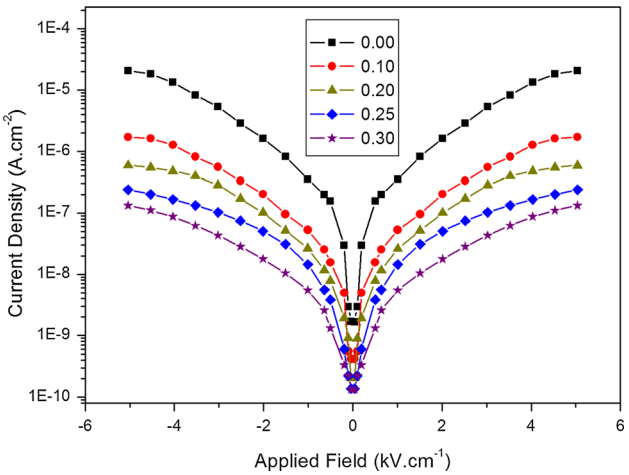

Fig. 3 Leakage current as a function of applied electrical field in $(1 - x)BiFeO_3$–$xBaTiO_3$ ceramics

The current density versus electric field (J–E) characteristics of the ceramics measured at room temperature are

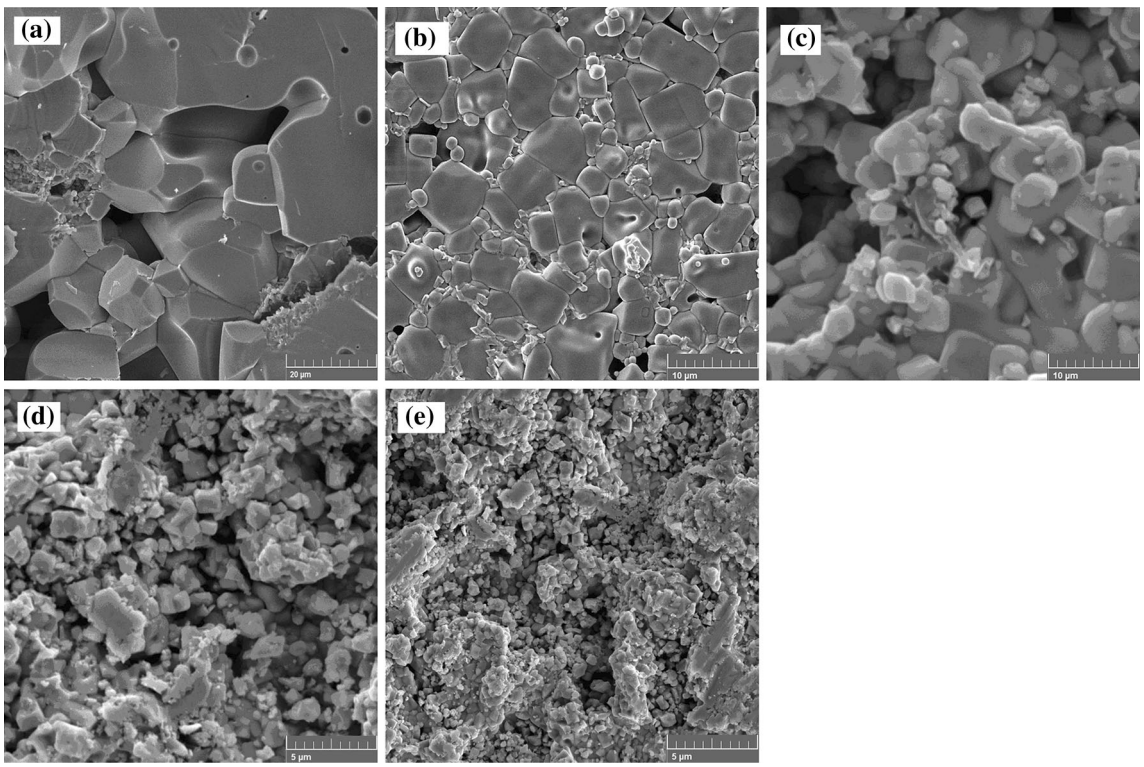

Fig. 2 SEM images of $(1 - x)BiFeO_3$–$xBaTiO_3$ samples **a** $x = 0.00$, **b** $x = 0.10$, **c** $x = 0.20$, **d** $x = 0.25$ and **e** $x = 0.30$

plotted in Fig. 3. It can be seen that the *J–E* curves of all samples display excellent symmetry under positive and negative electric fields, and the BTO doping significantly decrease the leakage current density of the ceramics. At the applied electric field of 5 kV/cm, the leakage current densities are 2.08×10^{-5}, 1.71×10^{-6}, 5.90×10^{-7}, 2.39×10^{-7} and 1.32×10^{-7} A/cm^2 for $x = 0.00$, 0.10, 0.20, 0.25 and 0.30 samples, respectively. This means that the leakage current decreases monotonically with the increase of the BTO content. As far as we know, the high leakage current in BFO-based materials is attributed to the presence of oxygen vacancies and Fe^{2+} ions. Since the strength of Ba–O bond is higher than that of Bi–O bond [17], the substitution of Ba for Bi can decrease the volatilization of Bi, lower the concentration of oxygen vacancies and Fe^{2+} ions. On the other hand, Fe site substitution with high valence Ti^{4+} ions acts as a donor and again reduces Fe^{2+} ions and oxygen vacancies. Therefore, the BTO doping can reduce the leakage conduction, and the leakage current density decreases with increasing BTO concentration.

Figure 4 shows the room temperature ferroelectric hysteresis loops of $(1 - x)$BFO–xBTO ceramics. It can be seen that the shape of ferroelectric hysteresis loop can be improved by BTO doping. The maximum applied electric field for undoped BFO is about 15 kV/cm, which is due to the low breakdown fields. Although all the samples do not show saturated hysteresis loops due to higher leakage current and partial reversal of polarization, the ferroelectric properties of the BTO doped samples are significantly improved in comparison with that of undoped BFO. The remnant polarization value (Pr) is about 0.083, 0.704, 1.131, 1.598 and 1.989 uC/cm^2 for $x = 0.00$, 0.10, 0.20, 0.25 and 0.30 ceramic samples, respectively. The results reveal that BTO doping can improve the ferroelectric properties and the attainable polarizations. The improved ferroelectric properties in BTO doped samples are supposed to result from two main sources. One may be attributed to the reduced leakage current density, which favors improved the ferroelectric behavior of BTO-doped BFO. The other one may come from the suppressed oxygen vacancy concentrations, as oxygen vacancies can play a critical role in the pinning of polarization switching domains [18]. Oxygen vacancies usually accumulate near domain boundaries, hence can cause domain pinning and reduce the Pr value of the ferroelectrics. Therefore, the ferroelectric properties of $(1 - x)$BFO–xBTO ceramics increase with increasing BTO doping content.

Figure 5 shows the room temperature magnetization hysteresis (M–H) loops of the (1 − x)BFO–xBTO ceramics measured under a magnetic field of 20 kOe. The undoped BFO sample exhibits a linear magnetization dependence of the magnetic field, which indicates the antiferromagnetic nature of BFO ceramic [19]. However, the BTO doped samples exhibit a typical magnetic hysteresis loops, exemplifying the ferromagnetic ordering and weak magnetization in the ceramics. It means that the antiferromagnetism behavior of BFO is turned into a weak ferromagnetism state by addition of BTO. The appearance of hysteresis loop for BTO doped samples may be firstly due to the suppressed spiral spin structure and the change of the canting angle by a structural distortion [20]. It is known that BFO shows a spiral modulated spin structure that produces nearly zero net magnetization [6–8]. The spatially modulated spin order in the $(1 - x)$BFO–xBTO ceramics is suppressed due to the partial substitutions of Ba^{2+} for Bi^{3+}

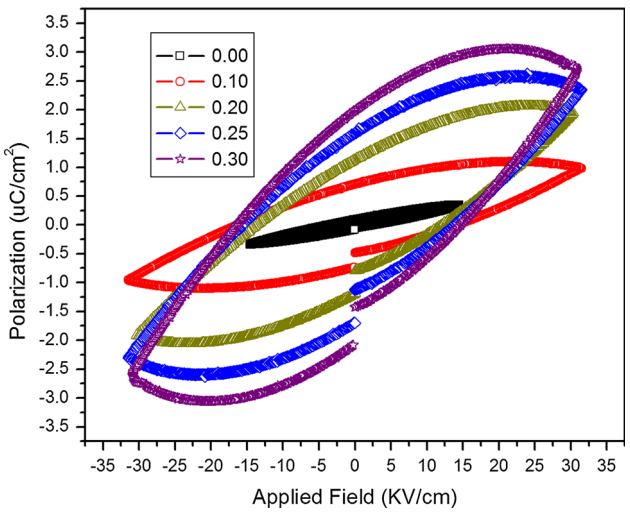

Fig. 4 The ferroelectric hysteresis loops of $(1 - x)BiFeO_3$–$xBaTiO_3$ ceramics at room temperature

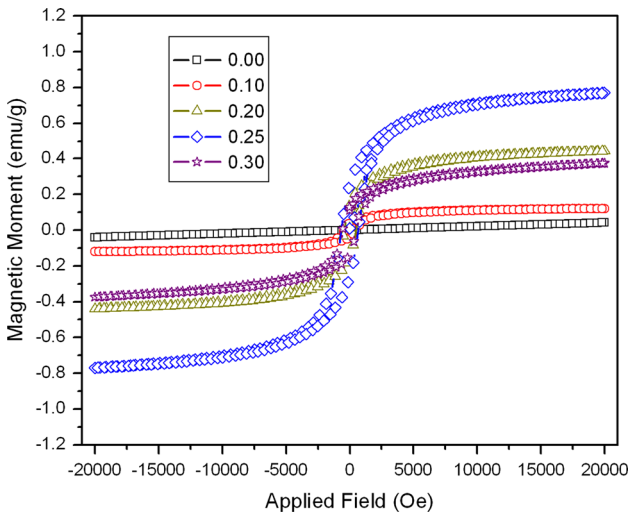

Fig. 5 The magnetization hysteresis loops of $(1 - x)BiFeO_3$–$xBaTiO_3$ samples at room temperature

and Ti^{4+} for Fe^{3+}, and thus releasing the locked magnetization [16, 20, 21]. Secondly, the substitution of Fe^{3+} spins by nonmagnetic Ti^{4+} breaks the balance between the two nearly antiparallel spins lattice of Fe^{3+}, and the neighboring spins cannot cancel out to each other producing a net magnetic moment (e.g. unbalanced Fe^{3+} spins) [11, 22, 23]. The values of saturation magnetization (Ms) for $x = 0.10$, 0.20, 0.25 and 0.30 samples are about 0.121, 0.442, 0.770 and 0.374 emu/g, respectively, and the values of remnant magnetization (Mr) are 0.042, 0.155, 0.269 and 0.140 emu/g, respectively. This means that the values of Ms and Mr increase with increasing BTO concentration from 0.00 to 0.25, then decrease with further increasing x. The decrease in measured remnant magnetization for $x = 0.30$ composition may be due to the decrease in the concentration of magnetic Fe^{3+} with the increase of BTO concentration [11]. This seems to be the optimal composition to enhance the magnetic properties for $(1 - x)$BFO–xBTO ceramics.

4 Conclusions

In conclusion, $(1 - x)$BFO–xBTO polycrystalline ceramics were fabricated by solid state reaction method, and the influences of BTO doping in the BFO compound on its structural, ferroelectric and magnetic behaviors were investigated. Several features can be concluded as follows:

1. BTO doping can induce the structure transition and hinder the formation of impurity phases;
2. BTO doping can hinder the grain growth;
3. BTO doping can effectively reduce the leakage current density of BFO ceramics.
4. BTO doping can effectively enhance the ferroelectric properties of BFO ceramics, and the remnant polarization increases with increasing BTO doping content.
5. The BFO-doped samples have a weak ferromagnetism. The values of saturation magnetization and remnant magnetization increase with increasing BTO content from 0.00 to 0.25, while decrease with further increasing BTO concentration.
6. The present study indicates that the BTO-doped BFO will have great potential applications.

Acknowledgments This work is supported by the National Natural Science Foundation of China (Nos. 11305142, 11175159), Zhengzhou Administration of Science and Technology of Henan Province of China (No. 131PPTGG411-10), and Key Members of the Outstanding Young Teacher of Zhengzhou University of Light Industry.

References

1. K. Chakrabarti, K. Das, B. Sarkar, S. Ghosh, S.K. De, G. Sinha, J. Lahtinen, Appl. Phys. Lett. **101**, 042401 (2012)
2. M. Kumar, S. Shankar, O. Parkash, O.P. Thakur, J. Mater. Sci.: Mater. Electron. **25**, 888 (2014)
3. J.G. Wu, J. Wang, D.Q. Xiao, J.G. Zhu, ACS Appl. Mater. Interfaces **4**, 1182 (2012)
4. F. Azough, R. Freer, M. Thrall, R. Cernik, F. Tuna, D. Collison, J. Eur. Ceram. Soc. **30**, 727 (2010)
5. S. Pattanayak, R.N.P. Choudhary, D. Pattanayak, J. Mater. Sci.: Mater. Electron. **25**, 3854 (2014)
6. J.L. Xu, D. Xie, C. Yin, T.T. Feng, X.W. Zhang, G. Li, H.M. Zhao, Y.F. Zhao, S. Ma, T.L. Ren, Y.J. Guan, X.S. Gao, Y.G. Zhao, J. Appl. Phys. **114**, 154103 (2013)
7. M. Kumar, P.C. Sati, S. Chhoker, J. Mater. Sci.: Mater. Electron. **25**, 5366 (2014)
8. J. Liu, M.Y. Li, L. Pei, J. Wang, Z.Q. Hu, X. Wang, X.Z. Zhao, EPL **89**, 57004 (2010)
9. R. Rai, I. Bdikin, M.A. Valente, A.L. Kholkin, Mater. Chem. Phys. **119**, 539 (2010)
10. Q.M. Hang, Z.B. Xing, X.H. Zhu, M. Yu, Y. Song, J.M. Zhu, Z.G. Liu, Ceram. Int. **38S**, S411 (2012)
11. H. Singh, A. Kumar, K.L. Yadav, Mater. Sci. Eng., B **176**, 540 (2011)
12. H. Dai, Z. Chen, R. Xue, T. Li, H. Liu, Y. Wang, Appl. Phys. A **111**, 907 (2013)
13. C. Yang, J.S. Jiang, C.M. Wang, W.G. Zhang, J. Phys. Chem. Solids **73**, 115 (2012)
14. X.J. Xi, S.Y. Wang, W.F. Liu, H.J. Wang, F. Guo, X. Wang, J. Gao, D.J. Li, J. Magn. Magn. Mater. **355**, 259 (2014)
15. M. Kumar, S. Shankar, R.K. Kotnala, O. Parkash, J. Alloy. Compd. **577**, 222 (2013)
16. P.C. Sati, M. Arora, S. Chauhan, M. Kumar, S. Chhoker, Ceram. Int. **40**, 7805 (2014)
17. J.A. Dean, *Lange's handbook of chemistry* (McGraw-Hill, New York, 1999)
18. Y. Li, J. Yu, J. Li, C. Zheng, Y. Wu, Y. Zhao, M. Wang, Y. Wang, J. Mater. Sci.: Mater. Electron. **22**, 323 (2011)
19. P. Sharma, V. Verma, J. Magn. Magn. Mater. **374**, 18 (2015)
20. R.A.M. Gotardo, D.S.F. Viana, M. Olzon-Dionysio, S.D. Souza, D. Garcia, J.A. Eiras, M.F.S. Alves, L.F.C. otica, I.A. Santos, A.A. Coelho, J. Appl. Phys. **112**, 104112 (2012)
21. Z.Z. Ma, Z.M. Tian, J.Q. Li, C.H. Wang, S.X. Huo, H.N. Duan, S.L. Yuan, Solid State Sci. **13**, 2196 (2011)
22. S.A. Ivanov, P. Nordblad, R. Tellgren, C. Ritter, Solid State Sci. **12**, 115 (2010)
23. F.P. Gheorghiu, A. Ianculescu, P. Postolache, N. Lupu, M. Dobromir, D. Luca, L. Mitoseriu, J. Alloy. Compd. **506**, 862 (2010)